Flow visualization in the wake of flapping-wing MAV 'DelFly II' in forward flight

M. Percin[1], H.E. Eisma[2], B.W. van Oudheusden[3], B. Remes [4], R. Ruijsink[5] , C. de Wagter[6]
Delft University of Technology, Kluyverweg 1, 2629 HS, Delft, The Netherlands

Time-resolved velocity field measurements in the wake of the flapping wings of the DelFly II Micro Aerial Vehicle (MAV) in forward flight configuration were obtained by Stereoscopic Particle Image Velocimetry (Stereo-PIV). The PIV measurements were performed at several spanwise planes in the wake of the flapping wings and at a high framing rate to allow a reconstruction of the temporal development of the three dimensional wake structures throughout the flapping cycle. The wake reconstruction was performed by interpolating between the measurement planes through a Kriging interpolation procedure. First, the general wake topology of the DelFly II model is described in conjunction with the behavior of the distinctive flow structures, in particular, tip vortex, trailing edge vortex, and root vortex. Second, the effect of reduced frequency is investigated by changing the flapping frequency. Comparison of the three dimensional wake structures for different cases of reduced frequency reveals major differences in both formation and interaction of vortical structures.

Nomenclature

c	=	mean chord length
f	=	flapping frequency
k	=	reduced frequency ($\pi f c/U_\infty$)
LEV	=	leading edge vortex
RV	=	root vortex
TEV	=	trailing edge vortex
TV	=	tip vortex
U_∞	=	free-stream velocity
$\|w_{xy}\|$	=	vorticity magnitude of only x and y component of vorticity
w_z	=	streamwise (z) component of vorticity
τ	=	non-dimensional time (non-dimensionalized with the period of the motion)

Indices

b	=	bottom wing
in	=	instroke
out	=	outstroke
t	=	top wing

---

[1] Ph.D. Student, Faculty of Aerospace Engineering, Aerodynamics Section, m.percin@tudelft.nl, Member AIAA.

[2] Graduate student, Faculty of Aerospace Engineering, Aerodynamics Section, h.e.eisma@student.tudelft.nl.

[3] Associate professor, Faculty of Aerospace Engineering, Aerodynamics Section, b.w.vanoudheusden@tudelft.nl.

[4] Research Associate, Faculty of Aerospace Engineering, MAV Laboratory, b.d.w.remes@tudelft.nl.

[5] Research Associate, Faculty of Aerospace Engineering, MAV Laboratory, h.m.ruijsink@tudelft.nl.

[6] Research Associate, Faculty of Aerospace Engineering, MAV Laboratory, c.dewagter@tudelft.nl.

I. Introduction

Flapping wing flight has attracted increased interest among aerodynamics researchers recently in view of the recent expansion of design efforts in the field of Micro Aerial Vehicles (MAVs). MAVs are given specific attention because of their potential as mobile platforms capable of reconnaissance and gathering intelligence in hazardous and physically inaccessible areas. To achieve these missions, they should be maneuvering with ease, staying aloft and propelling themselves efficiently. Conventional means of aerodynamic force generation are found lacking at this point and the flapping-wing approach, which has been improved in millions of years of evolution in nature, becomes an appealing or even necessary solution. In contrast to the conventional (fixed and rotary wing) force generation mechanisms, flapping wing systems take benefit from the unsteady flow effects that are associated to the vortices separating from the wing leading and trailing edges, which create low pressure regions around the wings that lead to the generation of higher lift and thrust[1].

DelFly II, which is the subject of investigation for the current paper, is a bio-inspired flapping wing MAV designed and built at Delft University of Technology. The DelFly has a bi-plane wing configuration (Fig. 1) with wings which consist of Mylar foil, reinforced with carbon rods. It has a total wing span of 280 mm, and weighs 17 g. A custom made brushless motor with a motor controller, a gear system and a crank shaft mechanism are used to drive the wings in flapping motion. A conventional cross-tail is used in order to guarantee stability and controllability. The DelFly can hover as well as fly in forward and backward direction. An essential part of the DelFly MAV system is that it is equipped with a miniature onboard camera, not only for observational purposes but also for making autonomous flight possible by use of the image analysis software in the ground station.

Figure 1. DelFly II in flight

The DelFly flapping biplane wing configuration displays the so-called clap-and-fling phenomena, as a mean of additional thrust and lift production. This effect was first described by Weis-Fogh[2] as a novel lift enhancement mechanism observed in animal flight and which is based on wing-wing interaction that takes place at the wing stroke reversal. During this phase in the flapping cycle, the leading edges of the wings come together and they pronate about their leading edges until the gap between them is closed in the clap phase. The fling phase starts with supination about the trailing edges and continues with the translation of the wings. Experiments on insects revealed that use of clap-and-fling motion increases aerodynamic lift per unit flight muscle by 25% with respect to conventional flapping motions[3]. The underlying unsteady aerodynamic mechanisms for this increase have been reported as: 1) the attenuation of starting vortex at the onset of the fling (thus diminished Wagner effect) due to the interaction of opposing circulation of each wing[4]; 2) the downward momentum jet formed at the end of clap, when the air trapped between the wings is forced downwards; 3) generation of a massive leading edge vortex (LEV) at the onset of fling which was verified experimentally by Lehmann et al.[5] Furthermore, the flexibility of the wings was shown to be an important parameter for the clap-and-fling motion. With the effect of flexibility, the wings tend to stick together with the fling occurring more like a peel and clap more like a reverse peel[6]. From aerodynamic loading point of view, it was shown that flexibility increases lift and decreases drag[7]. The effect of flexibility in the wings of the DelFly and its effect on the aerodynamic performance has been investigated in a number of previous experimental studies. De Clercq[8] performed Stereo-PIV experiments in the vicinity of the flapping wings of the DelFly in hover condition with simultaneous thrust (viz. lift) measurements. She described the clap-and-peel type flapping motion of the DelFly wings and found that the LEV at the onset of the fling phase increases lift. Bruggeman[9] performed a wing optimization study which resulted in a 10% increase in thrust-to-drag ratio. Groen[10] compared the flow fields around the original and improved DelFly wings and described the different behavior of LEVs, linking them to changes in flexibility behavior.

The LEV is known to be a primary source of high lift forces for the flapping flight mechanism. In view of this, the formation and stability of the LEV is an important issue in terms of lift enhancement and the generation of the fluid-dynamic forces in general. Ellington et al.[11] showed that the LEV on the flapping wings of the hawkmoth (*Manduca sexta*) has the shape of a conical spiral which enlarges from root to tip with spanwise flow component. It was conjectured that this spanwise flow is essential for the stability of LEV as it advects the vorticity out of the wing

tip to the tip vortex and prevents the LEV to accumulate into a large vortex which has a tendency to separate from the leading edge. Measurements on the flapping DelFly wings also revealed the conical growth of the LEV from root to tip, up to approximately 86% of the wing span after which it is no longer observed[12]. Groen[10] speculated that at this point the LEV tube becomes connected to the tip vortex and is bent towards the trailing edge.

Notwithstanding that the measurements in the vicinity of the flapping wings of the DelFly have provided substantial insight in the aerodynamic and aeroelastic behavior of the DelFly wings, the wake structure still remains largely unresolved. Also, all previous flow measurements were performed on the DelFly in a quiescent ambient environment, thus simulating the hovering flight mode. Therefore, the present investigation directs its attention to the wake formation behind the DelFly in the forward flight regime, simulated by placing the DelFly in the wind tunnel. The wake structure behind the flapping wings of the DelFly can be expected to bear resemblance to the wake of flapping animal species. Extensive measurements have been performed in the wake of flapping wings of bats at the University of Lund, which have revealed the existence of closed-loop vortical structures during the flapping motion[13]. Muijres et al.[14] identified the aerodynamic features present in the wake of a *G. soricina* bat: the starting vortex, the tip vortex, the root vortex and a reversed vortex dipole (the latter structure may be formed during part of the upstroke when the wing is producing negative lift). They described formation of vortex loops as a result of interactions between these vortex structures during the flapping cycle.

It is clear that the wake structure of the flapping wings requires a detailed investigation, particularly for the DelFly case which has two wing pairs and a tail that is presumably interacting with the wake structures of the wings. Therefore, additionally to the general characterization of the time-dependent flapping-wing wake structure, the interaction between the flapping-wing wake and the tail for different tail positions and angles of attack is a further particular point of interest in the investigation.

II.   Experimental Setup and Data Processing

A. The Experimental Model and Setup

The experiments were performed in one of the low speed wind tunnels at the Aerodynamic Laboratory of Delft University of Technology (TUDelft). The wind tunnel has an open test section with cross-section dimensions of 600 mm x 600 mm. The measurements were performed for free-stream velocities in the range of 2-6 m/s. The Reynolds numbers based on the mean wing chord-length and free-stream velocity are in the range of 10000-30000.

A complete DelFly II model was positioned in the test section of the wind tunnel in forward flight configuration by means of a balance mechanism. The balance mechanism has 6 component force sensor (ATI Nano-17) and two brushed servo motors to change the pitch and yaw angles of the model. Experiments were conducted at four different angles of attack of 0˚, 5˚, 10˚, and 15˚.

In addition to the free-stream velocity and the angle of attack, also the flapping frequency of the DelFly wings was varied in the range of 6-12 Hz by use of a microcontroller system that was also utilized for the phase determination of the wings and synchronization of the PIV images. Furthermore, measurements were performed at different tail configurations, i.e. no tail, tail at 30 mm and 60 mm downstream from the wing trailing edge.

B. Time-resolved Stereo-PIV

High-speed stereo-PIV measurements were carried out in order to capture time-resolved three-component spanwise oriented planar velocity fields in the wake of flapping wings of the DelFly model. The arrangement of Stereo-PIV setup is shown in Fig. 2.

The flow was illuminated with a double pulse Nd:YLF laser (Quantronix Darwin Duo) with a wavelength of 527 nm. The laser sheet with a thickness of 4 mm was kept fixed at a certain position and the complete balance mechanism was
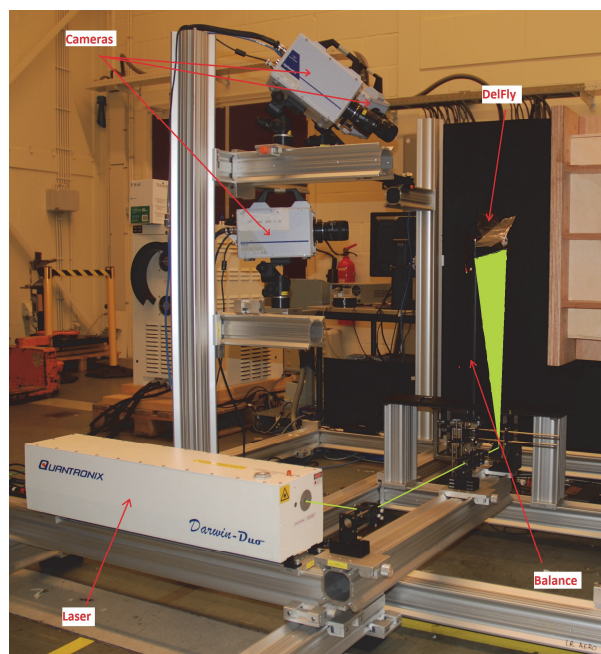

Figure 2. The Stereo-PIV setup

3
American Institute of Aeronautics and Astronautics

shifted in order to perform the measurement on a plane at a different streamwise position relative to the model. Measurements were performed at 12 consecutive planes with a distance of 10 mm in between each other (Fig. 3). The first measurement plane was placed 10 mm downstream from the trailing edge of the wings.

Water-glycol based fog of droplets with a mean diameter of 1µm, which is generated by SAFEX fox generator, was employed as tracer particles for the PIV measurements. In order to achieve homogenous seeding of the flow, the complete measurement room was filled with the fog beforehand.

Images of tracer particles were captured with three CMOS cameras with a maximum resolution of 1024x1024 pixels at 5.4 kHz. The pixel pitch of the cameras is 20 µm. Each camera was equipped with a Nikon 60 mm focal objective with numerical aperture of 4 for the first two cameras and 2.8 for the last camera and Scheimpflug adapters. It should be noted that the first two cameras, which were placed above the test section with an angle of 40° with respect to each other (Fig. 2), were primarily used for the stereo-PIV measurements. The third camera, which was placed at the same horizontal plane with the DelFly model, was utilized only when the tail caused considerable blockage in the view of the second camera. In that case, the first and the third cameras were employed for image acquisition, which were also placed at an angle of 40° with respect to each other.
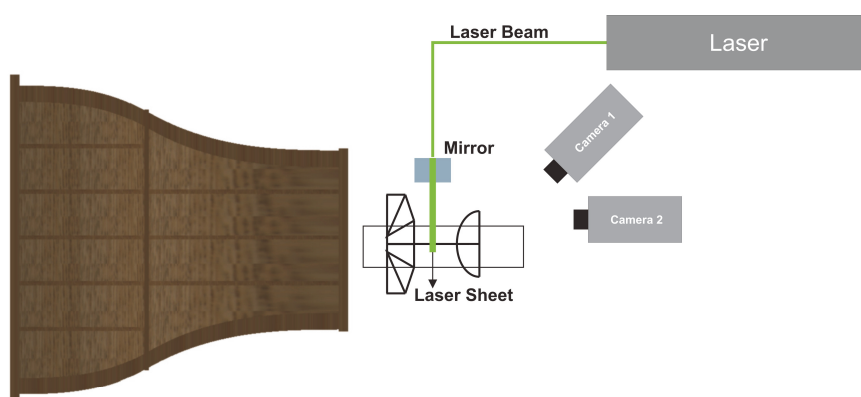

Figure 3. Sketch of the top view of the experimental setup

A field of view of 200 mm x 200 mm was captured with a magnification factor of approximately 0.1 at a digital resolution of 5 pixels/mm. Double frame image sequences of tracer particles were recorded with a recording frequency of 250 Hz. The time separation between two frames was 200 µs. Davis 8.0 (LaVision) was used in data acquisition, image pre-processing, stereoscopic correlation of the images, and further vector post-processing. The pre-processed double frame images were interrogated using windows of final size 64 pixels x 64 pixels with an overlap factor of 75% resulting in vector spacing of 3 mm in each direction.

C. Synchronization and Phase Determination

For the reconstruction of three dimensional wake structures, it is necessary to synchronize the PIV measurements with the flapping motion of the DelFly model. Thus, the images captured at the same phase of the flapping motion at different measurement planes can be determined and used for three dimensional reconstruction.

A microcontroller system was used in order to synchronize the stereo-PIV recordings with the flapping motion of the DelFly model. The system consists of two microcontrollers with inputs from the motor controller and a hall sensor with a magnet placed on the gear system of the DelFly model. It should be noted that the system also has other analog inputs (e.g. voltage and current form the motor controller) but they are out of the scope of the current study. The microcontroller system outputs a synchronization signal that consists of hall sensor data as an indication of the start of the period and the motor pulse data which is a precise indication of the phase of
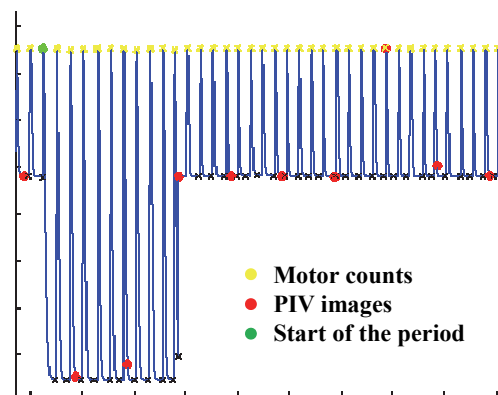

Figure 4. The synchronization signal captured via the microcontroller system

American Institute of Aeronautics and Astronautics

the flapping motion. After flapping for 100 periods based on the hall sensor input, the system also sends a trigger signal to the stereo-PIV system and image acquisition starts. By acquiring the synchronization signal at 25 kHz (Fig. 4), the synchronization of measurements at different planes was performed accurately.

On the other hand, it is necessary to find out the relation between the motor pulses and the stroke angle of the flapping wings in order to analyze the resultant three dimensional flow fields. Therefore, an additional measurement was performed, in which a high speed camera was positioned normal to the wings of the DelFly model in front view. The flapping motion of the wings was captured at a recording frequency of 2 kHz with the synchronization signal. Then, a dedicated Matlab script was used to detect the leading edges, to calculate the stroke angles of the wings (Fig. 5a) and to correlate it with the synchronization signal. Consequently, the phase distributions of the upper and lower wing during flapping for different frequencies were captured as shown in Fig. 5b.

a) **b)**
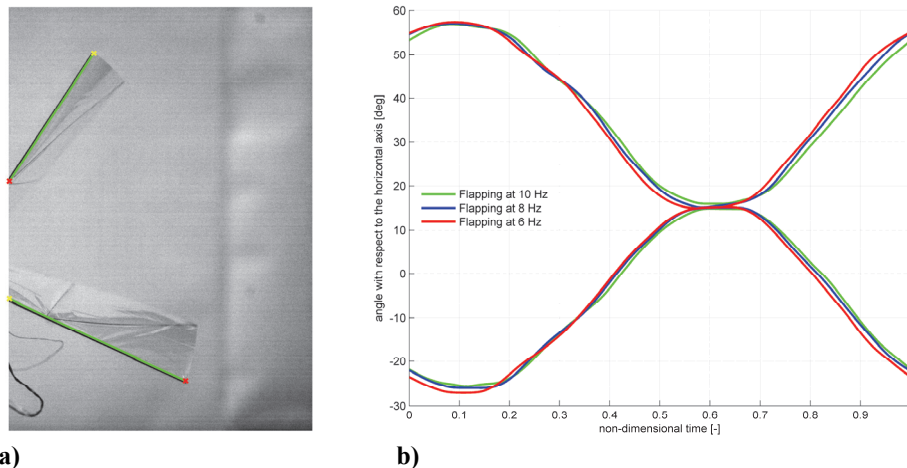
Figure 5. a) An example of leading edge detection during instroke b) Time variation of stroke angles of upper and lower wings during flapping motion at different frequencies. (Note that the mean value is non-zero as a consequence of the wing dihedral)

D. Interpolation

The flow fields from consecutive planes for the same flapping phase were subsequently interpolated to reconstruct the three dimensional wake of the flapping DelFly wings. The interpolation was performed by use of Kriging interpolation. Other interpolation techniques, i.e. linear, cubic, and spline interpolation, were also utilized and compared with the performance of the Kriging interpolation method. A detailed analysis of the comparative performance of the different methods is out of scope of the current study, however. Concisely, the Kriging interpolation technique is chosen in view of two prominent features: 1) the ability to work with unstructured data; 2) the capability of taking into account the measurement uncertainty. The first property is effectual for the current study as for different measurement planes, different masking geometries needed to be applied. In consequence, each velocity field used in the interpolation does not have necessarily the same number and structure of data points. Besides, the second property is of great importance for any kind of experimental data as it diminishes the effect of measurement points with higher uncertainty on the interpolated point. The Kriging estimator of unknown values x based on the given data y is formulized as follows[15];

$$E(x|y) = \mu + PH^T(R + HPH^T)^{-1}(y - H\mu) \tag{1}$$

Equation (1) is built up from a few different terms. First of all, the quantity μ is known as the mean base term, which is taken as the statistical mean of the observed data. H is the observation matrix. Furthermore, P is the covariance matrix containing three-dimensional Gaussian functions for the correlation between the data points. In order to limit the computational cost, frequency-domain sample variogram method is used to estimate the correlation lengths. A three dimensional Gaussian surface is fitted to the power spectrum of the data. The width, length and height of this surface provide a good approximation of the correlation lengths. Finally, R is the observation error covariance matrix.

In the current study, constant error approximation for each velocity component on the same plane was applied. The error was determined from a brute force minimization of the cross validated root-mean-square error. The cross

American Institute of Aeronautics and Astronautics

validation was performed on a sub-domain of the total volume and the value which maximized the contained signal power was selected. For further processing, the signal to noise ratio of the Stereo-PIV data will be utilized in the interpolation technique as an error approximation.

III. Results

As mentioned, experiments were performed for a large variety of parameters, i.e. flapping frequency, free-stream velocity, angle of attack and tail configuration. However, due to excessive amount of data to be processed and analyzed, and the complexity of the related aerodynamic phenomena, preliminary results are discussed in this section for a selection of parameter combinations. First, the vortex topology in the wake of the flapping wings is described and the way it is observed to evolve over a flapping cycle. Next, the effect of reduced frequency is addressed by comparing cases of different flapping frequencies. It should further be noted that only the cases 0° angle of attack and tail position of 30 mm downstream from the trailing edge are considered in the current paper.

A. Wake Topology

Wake vortex topology is described for the case of k=0.67 (f=8 Hz and U_∞=3 m/s). Before starting the description of vortex topology, it is necessary to define the methodology followed to define the flow structures and underline some important points regarding to interpretation of the results. First, it should be noted that only one half of the wake is visualized (the wake, however, is assumed to be nominally symmetrical) and that the region in the vicinity of the tail masked during PIV processing due to intensive reflection underneath and lack of illumination above the tail. Additionally, to assist the interpretation of the results, the DelFly wings are schematically displayed in the images as an indication of the flapping phase; however, they are represented as rigid bodies whereas in reality there is a significant amount of deformation on the wings during the flapping motion (Maximum trailing edge deformation with respect to rigid leading edge is 60% of the mean chord length[16]). Therefore, the position of vortical structures may occasionally seem to be uncorrelated with the position of the wings. Regarding to the definition of vortices, the terminology of leading and trailing edge vortices (LEV, TEV) shown in Fig. 6 is adopted. Iso-surfaces of vorticity magnitude are used to visualize vortical flow structures. Additional detailed analysis, which is not represented in this paper, was performed to define and label vortical structures based on their direction of rotation and time of advection. For the wake topology section, the isovalue for the drawings is set to 0.125s^{-1}.
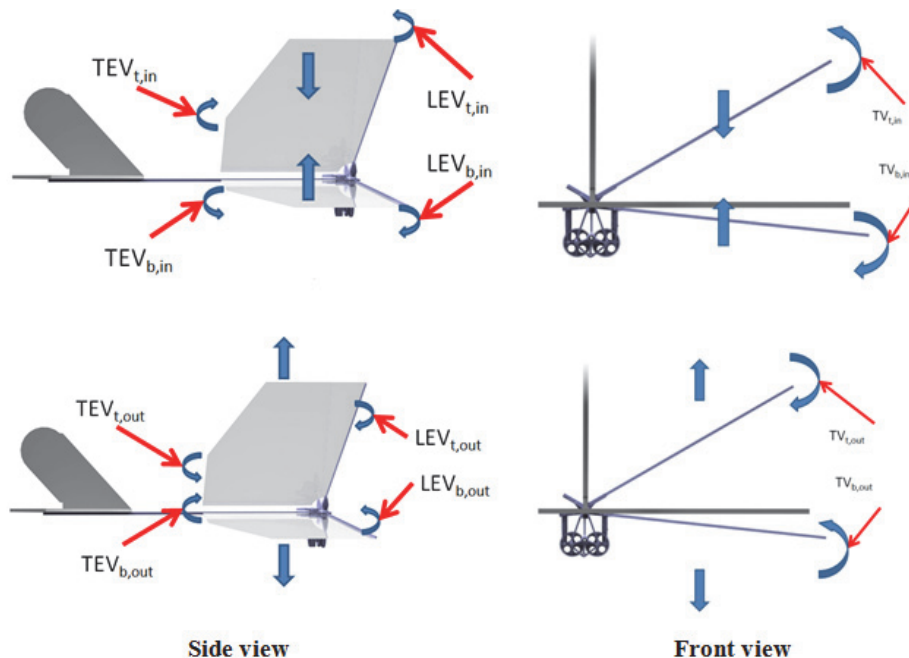
**Figure 6. Vortex definitions for instroke (top) and outstroke (bottom)**

The start of the flapping motion is defined at the beginning of the instroke. As the reconstructed volume starts 10 mm downstream of the trailing edge, it takes some time to observe stroke reversal structures inside the measurement

volume. The iso-surfaces of vorticity magnitude at the non-dimensional time of 0.17 are shown in Fig. 7. Two tip vortices (one from each wing) generated during the previous outstroke are present in the reconstructed volume at this time instant. It is clear that the lower tip vortex ($TV_{b,out}$) is stronger and more coherent than the upper tip vortex ($TV_{t,out}$) which has a swirling shape. It is assumed that this asymmetry of the vortical structures can be attributed to the dihedral angle of the wings.
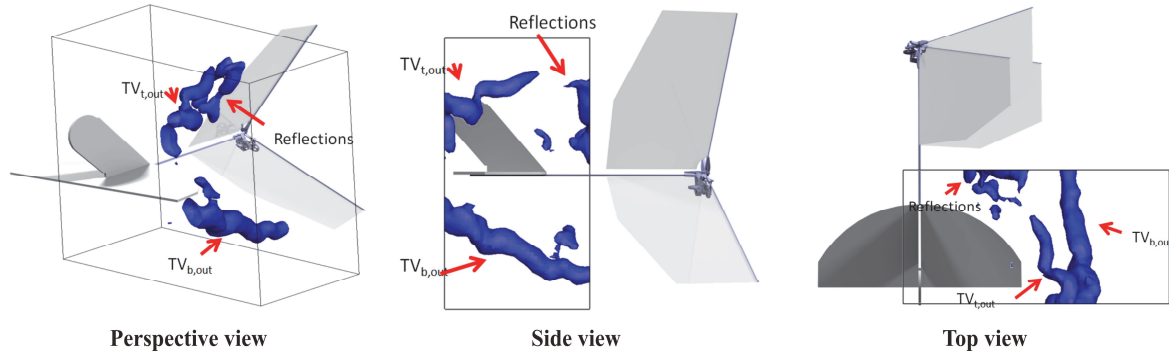
Figure 7. Iso-surfaces of vorticity magnitude at τ=0.17 for the case of k=0.67 (f=8 Hz and U∞=3 m/s)

Moving to the time step of τ=0.31 (Fig. 8), the flow structures of the new stroke have become visible in the field of view. It is clear that initially trailing edge vortices of upper and lower wings are shed downstream ($TEV_{t,in}$ and $TEV_{b,in}$). It is also observed that the vortical structures of the consecutive strokes are disconnected from each other. It can be speculated that the discontinuity of vorticity in the wake can create unsteadiness in the induced velocity that can affect the lift generation of tail.
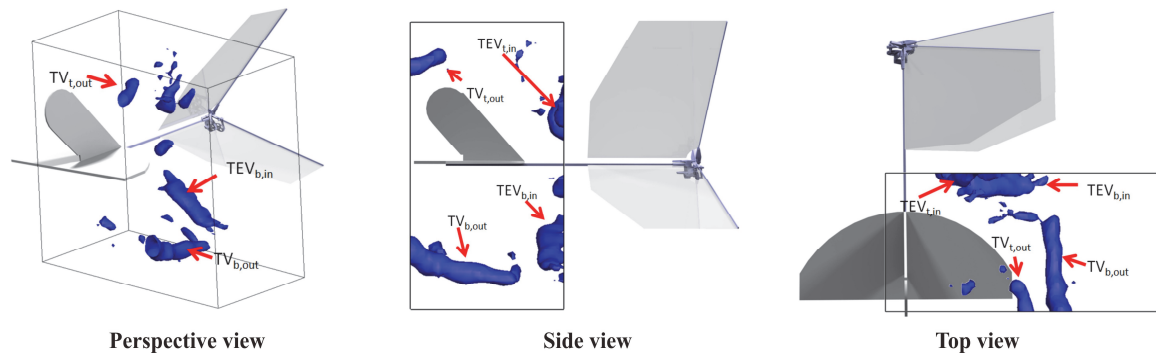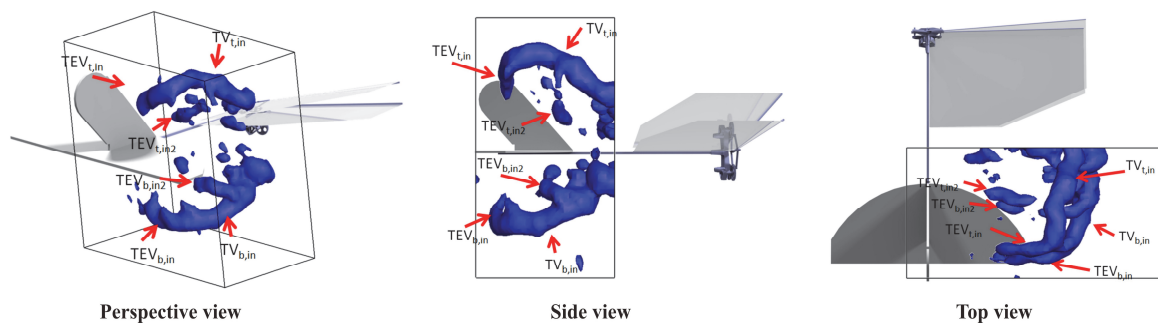

Figure 8. Iso-surfaces of vorticity magnitude at τ=0.31 for the case of k=0.67 (f=8 Hz and U∞=3 m/s)

At the time step of τ=0.37 (Fig. 9), U-shaped vortical structures downstream of both upper and lower wings appear in the field of view. The U-shaped vortical structure is formed as a result of connection between the tip vortex of the instroke phase, the trailing edge vortex shed during the stroke reversal and the root vortex formed during instroke.

American Institute of Aeronautics and Astronautics
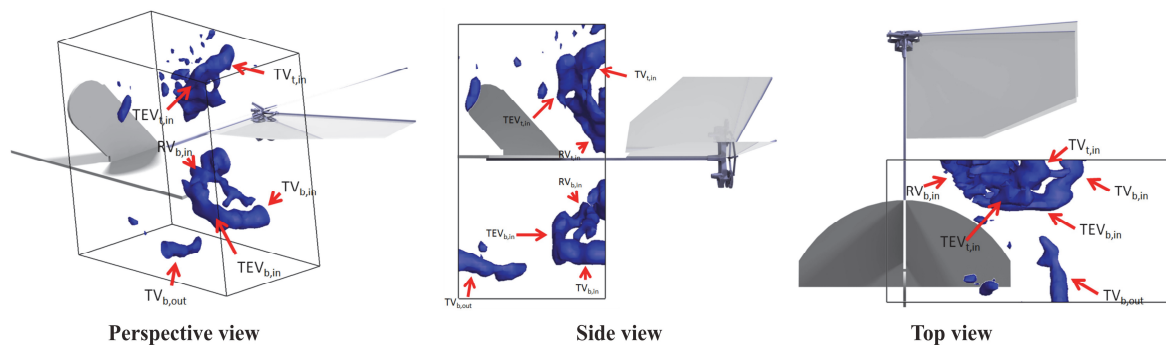
Figure 9. Iso-surfaces of vorticity magnitude at τ=0.37 for the case of k=0.67 (f=8 Hz and U∞=3 m/s)

The iso-surfaces of vorticity magnitude at the end of instroke (τ=0.5) are shown in Fig. 10. It is clear that the root vortex is not present at the root of the wings as the wings clap at this time instant. The trailing edge vortices of both wings (TEV$_{t,in}$ and TEV$_{b,in}$), on the other hand, keep their connection with the tip vortices (TV$_{t,in}$ and TV$_{b,in}$) and are advected downstream.

Figure 10. Iso-surfaces of vorticity magnitude at τ=0.5 for the case of k=0.67 (f=8 Hz and U∞=3 m/s)

In the following figures, the outstroke phase of the flapping motion is examined. At the time step of τ=0.72 (Fig. 11), upper and lower tip vortices of the previous instroke are being advected downstream while interacting with each other. Contrary to the start of instroke, a trailing edge vortex (TEV$_{t,out}$) is generated only at the outer part of the wing as the inner parts (closer to root) are still attached to each other (as evidenced from high-speed visualization of the wing deformation). Ideally, no starting vortex is expected to be generated in the clap-and-fling type flapping motion as the bound vorticity of each wing acts as the starting vortex for the other. The gap between the vortical structures of consecutive strokes is smaller at the stroke reversal from instroke to outstroke, than for the reversal from outstroke to instroke (see Fig.8).
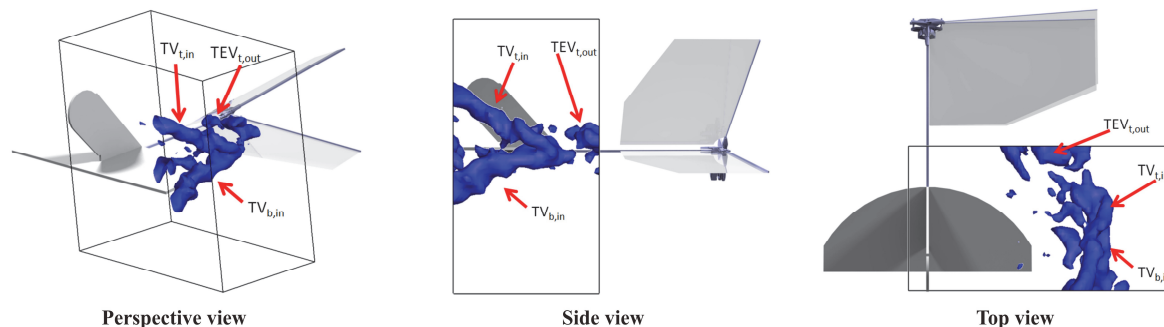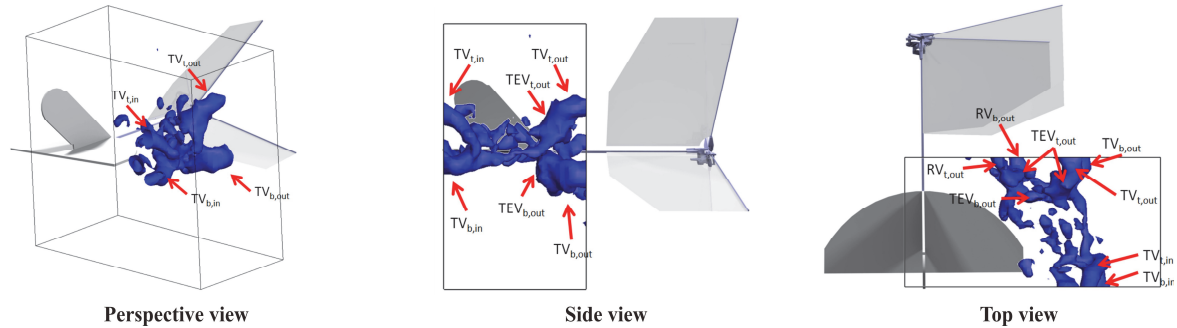

Figure 11. Iso-surfaces of vorticity magnitude at τ=0.72 for the case of k=0.67 (f=8 Hz and U∞=3 m/s)

Moving to the time step of τ=0.8 (Fig. 12), it can be observed that again a U-shaped structure is present in the wake of the wings. This time however, the structure is smaller in spanwise extent and positioned only at the tapered

outer part of the wings, as closer to the root the wings are still attached to each other. This causes the root vortices ($RV_{t,out}$ and $RV_{b,out}$) to be formed at the location of the wing stiffeners instead of at the actual wing root. The root vortices are connected to newly formed tip vortices ($TV_{t,out}$ and $TV_{b,out}$) by means of trailing edge vortices ($TEV_{t,out}$ and $TEV_{b,out}$).
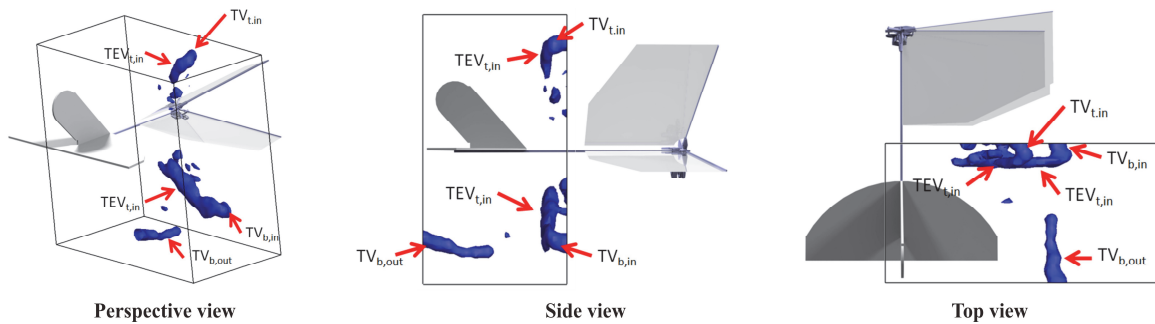

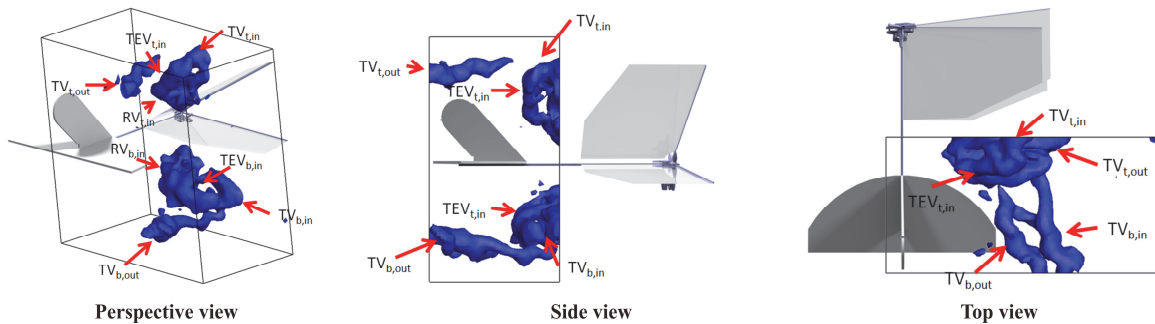**Figure 12. Iso-surfaces of vorticity magnitude at τ=0.80 for the case of k=0.67 (f=8 Hz and U∞=3 m/s)**

B. Effect of Reduced Frequency

In order to investigate the effect of reduced frequency, the flapping frequency is increased to 12 Hz while keeping the free-stream velocity fixed (k=1). The resultant flow structures are compared by means of vorticity magnitude with isovalue of 0.15 s^{-1}. The latter is performed to visualize the structures of higher reduced frequency case clearly. In addition, vorticity magnitude of only x and y component of vorticity with separately z vorticity are utilized to distinguish the components of vortical structures.

First, two different reduced frequency cases are compared by means of Fig. 13 and Fig.14 at the time instant of τ=0.31.

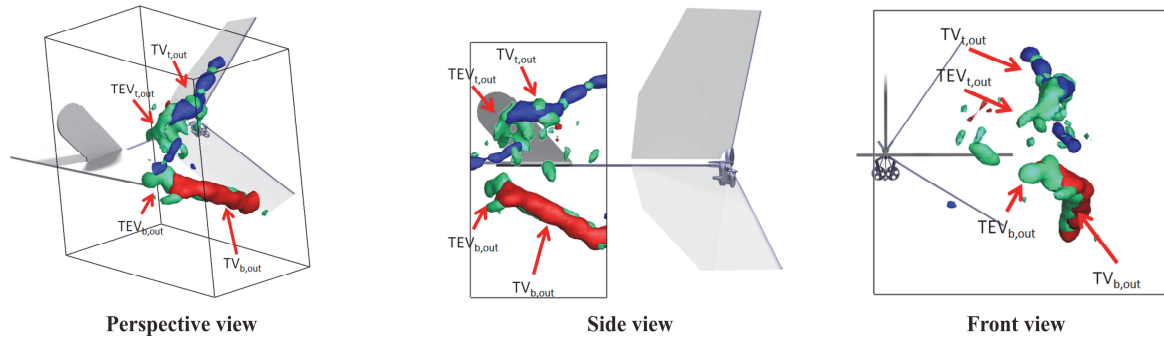**Figure 13. Iso-surfaces of vorticity magnitude at τ=0.31 for the case of k=0.67 (f=8 Hz and U∞=3 m/s)**

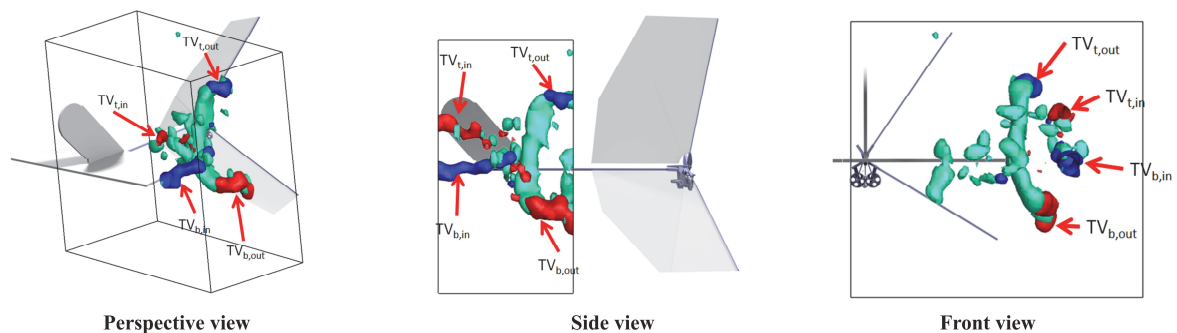**Figure 14. Iso-surfaces of vorticity magnitude at τ=0.31 for the case of k=1 (f=12 Hz and U∞=3 m/s)**

The vortical structures for the case of k=1 are stronger and more coherent when compared to the lower reduced frequency. The difference in strength is so dramatic that at k=0.67, the upper tip vortex of the previous (out)stroke

9
American Institute of Aeronautics and Astronautics

($TV_{t,out}$) cannot be visualized at this isovalue whereas the tip vortices of the higher reduced frequency case can be visualized clearly. It is not surprising as the amount of energy transferred to the flow by the flapping motion is larger at the higher frequency case. Furthermore, for the case of k=0.67, the vortical structures are advected downstream relatively parallel to the free stream, however an increasing reduced frequency introduces a path of the vortical structure that is more attracted towards the tail. At higher reduced frequencies, the possibility of wake-tail interaction therefore increases. Another important difference is the decrease of the gap between flow structures of consecutive strokes that will change the characteristics of induced velocity region close to the tail as well.

Moving to time instant of τ=0.92 reveals another dramatic effect of reduced frequency. For this time instant, vorticity magnitude of x and y component and z vorticity are plotted separately (Fig. 15 and Fig.16).
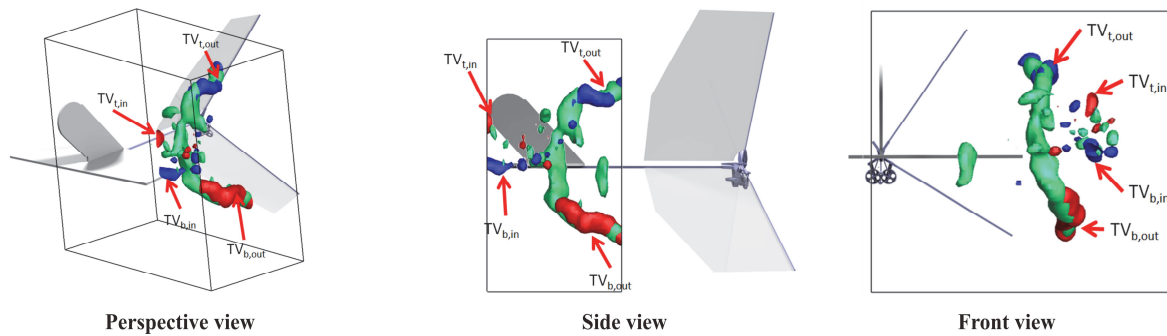

Figure 15. Iso-surfaces of vorticity magnitude $|w_{xy}|$ combined with w_z at τ=0.92 for the case of k=0.67 (f=8 Hz and U_∞=3 m/s). The isovalues of $|w_{xy}|$ and w_z are 0.15 s^{-1} and ±0.125 s^{-1}, respectively. Blue color represents clockwise z vorticity and red color represents counterclockwise z vorticity. Green colored surfaces stand for $|w_{xy}|$ iso-surfaces.

Figure 16. Iso-surfaces of vorticity magnitude $|w_{xy}|$ combined with w_z at τ=0.92 for the case of k=1 (f=12 Hz and U_∞=3 m/s). The isovalues of $|w_{xy}|$ and w_z are 0.2 s^{-1} and ±0.20 s^{-1}, respectively. Blue color represents clockwise z vorticity and red color represents counterclockwise z vorticity. Green colored surfaces stand for $|w_{xy}|$ iso-surfaces.

It is clear from these figures that the tip vortices of outstroke ($TV_{t,out}$ and $TV_{b,out}$) at this time instant are connected to each other via a vortex tube rotating about the vertical axis for the higher reduced frequency case. There is also such a tendency of interaction between tip vortices at lower reduced frequency case but it does not occur as free-stream is relatively more dominant than in the of case k=1. This vertical closed loop structure maintains its shape during the outstroke (Fig. 17) and early instroke (Fig. 18) and possibly interacts with the tail.

| Perspective view | Side view | Front view |

Figure 17. Iso-surfaces of vorticity magnitude $|w_{xy}|$ combined with w_z at τ=0.99 for the case of k=1 (f=12 Hz and U_∞=3 m/s). The isovalues of $|w_{xy}|$ and w_z are 0.2 s^{-1} and ±0.20 s^{-1}, respectively. Blue color represents clockwise z vorticity and red color represents counterclockwise z vorticity. Green colored surfaces stand for $|w_{xy}|$ iso-surfaces.

| Perspective view | Side view | Front view |
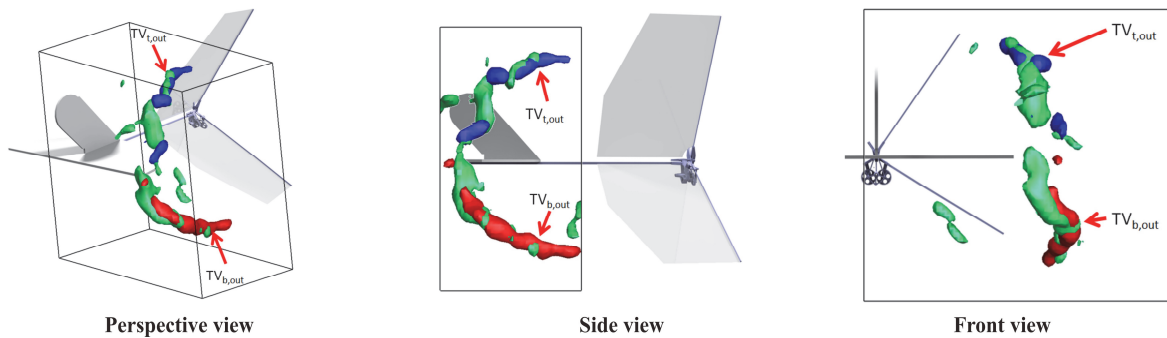
Figure 18. Iso-surfaces of vorticity magnitude $|w_{xy}|$ combined with w_z at τ=0.17 for the case of k=1 (f=12 Hz and U_∞=3 m/s). The isovalues of $|w_{xy}|$ and w_z are 0.2 s^{-1} and ±0.20 s^{-1}, respectively. Blue color represents clockwise z vorticity and red color represents counterclockwise z vorticity. Green colored surfaces stand for $|w_{xy}|$ iso-surfaces.

IV. Conclusion

In this study, the three-dimensional time-resolved wake of the flapping wings of the DelFly II is reconstructed from time-resolved Stereo-PIV measurement performed at consecutive spanwise oriented measurement planes. The experiments were performed for a variety of parameters, which are flapping frequency, free stream velocity, angle of attack of the DelFly and tail configuration. Preliminary results are discussed in this paper due to the restriction of the extensive time required to process and to analyze the data available.

First, the wake topology is described in detail for one particular flapping configuration. Flow structures and their formation and evolution during the flapping cycle are described. The effect of reduced frequency is subsequently investigated by changing the flapping frequency. It was observed that by increasing the reduced frequency, the behavior of flow structures changes significantly. Notwithstanding the valuable new insights gained by these preliminary results, a further detailed analysis and study of the additional cases that were measured is necessary to support any more definite conclusions regarding the complicated three-dimensional aerodynamic phenomenon.

References

[1]Young, J., "Numerical simulation of the unsteady aerodynamics of flapping airfoils," Ph.D. Dissertation, The University of New South Wales, Sydney, 2005.

[2]Weis-Fogh, T., "Quick estimates of flight fitness in hovering animals, including novel mechanisms for lift production," *The Journal Experimental Biology*, Vol. 59, 1973, pp. 169-230.

[3]Marden, J., "Maximum lift production during take-off in flying animals," *The Journal of Experimental Biology*, Vol. 130, 1987, pp. 235–258.

[4]Sane, S.P., "The aerodynamics of insect flight," *The Journal of Experimental Biology*, Vol. 206, Aug. 2003, pp. 4191-4208.

[5]Lehmann, F.O., Sane, S.P., Dickinson, M., "The aerodynamic effect of wing-wing interaction in flapping insect wings," *The Journal of Experimental Biology*, Vol. 208, 2005, pp. 3075-3092.

[6]Ellington, C.P., "The aerodynamics of insect flight. IV. Aerodynamic mechanisms," *Philosophical Transactions of the Royal Society B.*, Vol. 305, 1984, pp. 79–113.

[7]Miller, L.A., Peskin, C.S., "Flexible clap and fling in tiny insect flight," *The Journal of Experimental Biology*, Vol. 212, June 2009, pp. 3076-3090.

[8]De Clercq, K.M.E., "Flow visualization and force measurements on a hovering flapping wing MAV DelFly II," M.Sc. thesis, Delft University of Technology, Delft , 2009.

[9]Bruggeman, B., "Improving flight performance of DelFly II in hover by improving wing design and driving mechanism," M.Sc. thesis, Delft University of Technology, Delft , 2010.

[10]Groen, M., "PIV and force measurements on the flapping-wing MAV DelFly II", M.Sc. thesis, Delft University of Technology, Delft, 2010.

[11]Ellington, C.P., Van den Berg, C., Willmott, A.P., Thomas, A.L.R., "Leading-edge vortices in insect flight," *Nature*, Vol. 384, Dec. 1996, pp. 626-630.

[12]Groen, M., Bruggeman, B., Remes, B.W., Ruijsink, R., Oudheusden, B., Bijl, H., "Improving flight performance of the flapping wing MAV DelFly II", *IMAV Conference*, Braunschweig, 2010.

[13]Hubel, T.Y., Hristov, N.I., Swartz, S.M., Breuer, K.S. "Time-resolved wake structure and kinematics of bat flight," *Experiments in Fluids*, Vol. 46, No.5, 2009, pp. 933-943.

[14]Muijres, F.T., Spedding, G.R., Winter, Y., Hedenström, A., "Actuator disk model and span efficiency of flapping flight in bats based on time-resolved PIV measurements," *Experiments in Fluids*, Vol. 51, No. 2, 2011, pp. 511-525.

[15]Wikle, C.K., Berliner, L.M., "A Bayesian tutorial for data assimilation," *Physica D*, Vol. 230, No. 1-2, 2007.

[16]Percin, M., Hu, Y., van Oudheusden, B.W., Remes, B., Scarano, F., "Wing flexibility effects in clap-and-fling," *International Journal of Micro Air Vehicles,* Vol. 3, No. 4, Dec. 2011, pp. 217-227.